ADVANCED FUNCTIONAL MATERIALS
www.afm-journal.de

Walnut-Like Multicore–Shell MnO Encapsulated Nitrogen-Rich Carbon Nanocapsules as Anode Material for Long-Cycling and Soft-Packed Lithium-Ion Batteries

Guoyin Zhu, Lei Wang, Huinan Lin, Liaobo Ma, Peiyang Zhao, Yi Hu, Tao Chen, Renpeng Chen, Yanrong Wang, Zuoxiu Tie, Jie Liu, and Zhong Jin**

Metal oxide-based nanomaterials are widely studied because of their high-energy densities as anode materials in lithium-ion batteries. However, the fast capacity degradation resulting from the large volume expansion upon lithiation hinders their practical application. In this work, the preparation of walnut-like multicore–shell MnO encapsulated nitrogen-rich carbon nanocapsules (MnO@NC) is reported via a facile and eco-friendly process for long-cycling Li-ion batteries. In this hybrid structure, MnO nanoparticles are uniformly dispersed inside carbon nanoshells, which can simultaneously act as a conductive framework and also a protective buffer layer to restrain the volume variation. The MnO@NC nanocapsules show remarkable electrochemical performances for lithium-ion batteries, exhibiting high reversible capability (762 mAh g^{-1} at 100 mA g^{-1}) and stable cycling life (624 mAh g^{-1} after 1000 cycles at 1000 mA g^{-1}). In addition, the soft-packed full batteries based on MnO@NC nanocapsules anodes and commercial $LiFePO_4$ cathodes present good flexibility and cycling stability.

1. Introduction

Rechargeable lithium-ion batteries (LIBs) have been widely used as the power sources to fulfill the demands for portable electronics and electric vehicles because of the high-energy density and long cycling life.[1–4] However, due to the low theoretical capacity (372 mAh g^{-1}) of graphitic carbon anodes, the commercial LIBs are nearly reaching the performance limitation.[5] Thus, extensive efforts have been dedicated to developing advanced anode materials with higher capacity, such as IVA-group materials,[6–8] metal sulfides,[9–11] and metal oxides.[12–15] Metal oxides, such as MnO_x,[16–27] have attracted much attention as potential anode materials due to the low electromotive force value, high theoretical capacity, as well as their environmental friendliness and abundance. Nevertheless, there are two major issues that impede their application: (1) The inferior electronic conductivity of metal oxides is unfavorable for the electrochemical lithium ion insertion/extraction reactions. (2) The drastic volume change during the charge–discharge cycles leads to pulverization of metal oxides and also poor cyclability.[16–21] Therefore, the rational design and realization of hybrid nanostructures are required to improve the electrochemical performances. To this end, intensive attention has been paid to the controllable nanoengineering of metal oxide-based ultrafine nanostructures.[22–25,28,29] These nanostructures can improve the contacts of electrode–electrolyte interface, shorten the path for lithium-ion diffusion within active material particles, and alleviate the structural strain of volume change during the repeating Li^+ insertion/extraction processes. An efficient strategy is the construction of well-organized composites integrated by nanostructured metal oxides and carbon materials.[26,27,30,31] The carbon materials can enhance the conductivity, prevent the pulverization of active material nanoparticles, and decrease the undesirable side reactions between the electrode and electrolyte. However, this strategy usually involves complicated preparation and structure control processes for the composite electrode materials. It remains a challenge to develop a facile and universal approach to prepare uniform metal oxide nanoparticles encapsulated carbon frameworks with desirable compositions and morphologies.

In this work, we propose a facile method that incorporates a hydrothermal reaction step and a following heating step to prepare ultrafine MnO nanoparticles encapsulated nitrogen-rich carbon nanocapsules (MnO@NC) with walnut-like multicore–shell structure. In this approach, polyaniline (PANI) was used as carbon precursor, which can provide high content of nitrogen heteroatom doping, which is beneficial to the wettability and electronic conductivity of carbon shells. Meanwhile,

G. Zhu, L. Wang, H. Lin, L. Ma, P. Zhao, Y. Hu, Dr. T. Chen, R. Chen, Y. Wang, Dr. Z. Tie, Prof. J. Liu, Prof. Z. Jin
Key Laboratory of Mesoscopic Chemistry of MOE
School of Chemistry and Chemical Engineering
Nanjing University
Nanjing, Jiangsu 210023, China
E-mail: j.liu@duke.edu; zhongjin@nju.edu.cn
Prof. J. Liu
Department of Chemistry
Duke University
Durham, NC 27708, USA
The ORCID identification number(s) for the author(s) of this article can be found under https://doi.org/10.1002/adfm.201800003.

DOI: 10.1002/adfm.201800003

the PANI-derived carbon shells can effectively prevent the aggregation and pulverization of MnO nanoparticles. As expected, the MnO@NC nanocapsules with the synergistic advantages of uniformly dispersed MnO nanoparticles and conductive carbon shells exhibited remarkable lithium storage performances. Furthermore, soft-packed full batteries based on commercial $LiFePO_4$ cathodes and MnO@NC anodes showed remarkable flexibility and cycling stability.

2. Results and Discussion

The overall preparation route of walnut-like multicore–shell MnO@NC nanocapsules is detailed in the Experimental Section of the Supporting Information and schematically illustrated in **Figure 1**a, which involves two steps: (1) As an intermediate product, Mn_3O_4@PANI nanocapsules were first synthesized by a hydrothermal reaction step with a solution containing $KMnO_4$, $Mn(NO_3)_2$, and aniline. (2) The as-prepared Mn_3O_4@PANI nanocapsules were thermally treated in N_2 atmosphere to prepare MnO@NC nanocapsules. During the calcination, the Mn_3O_4 nanoparticles were reduced to MnO nanoparticles and the PANI shells were carbonized into N-doped carbon nanocapsules.

The morphologies of as-prepared Mn_3O_4@PANI intermediate product and MnO@NC nanocapsules were investigated by scanning electron microscopy (SEM) and transmission electron microscopy (TEM). The Mn_3O_4@PANI nanocapsules exhibited irregular shapes (Figure 1b). After calcination at 800 °C in N_2 atmosphere for 4 h, the MnO@NC nanocapsules were finally prepared, with the average size slightly smaller than the precursor Mn_3O_4@PANI nanocapsules (Figure 1c). The corresponding energy-dispersive X-ray spectrometry (EDX) elemental mappings (Figure 1d) display a uniform distribution of C, N, O, and Mn elements in MnO@NC nanocapsules. From the TEM images (Figure 1e–g), it could be seen that MnO nanoparticles with an average diameter of ≈15 nm were uniformly encapsulated and confined in the carbon nanoshells (Figure 1f), forming a walnut-like morphology. Such an intriguing nanostructure can efficiently improve the electrical conductivity and prevent the aggregation and breakage of MnO nanoparticles. A closer look from high-resolution TEM (HRTEM, Figure 1g) revealed an interplanar spacing of 0.26 nm, derived from the (111) planes of MnO.[27] After the etching of MnO cores by HCl solution (Figure S1a–c, Supporting Information), the morphology of hollow N-doped carbon nanoshells exhibited a uniform thickness of ≈5 nm, suggesting that the N-doped carbon nanoshells of MnO@NC nanocapsules were homogeneously coated on ultrafine MnO nanoparticles.

The crystalline structures of as-synthesized samples were investigated by X-ray powder diffraction (XRD). As shown in **Figure 2**a, the diffraction peaks of Mn_3O_4@PANI nanocapsules were assigned to tetragonal Mn_3O_4 (JCPDS No. 24–0734), where PANI showed no recognizable peak due to its polymeric

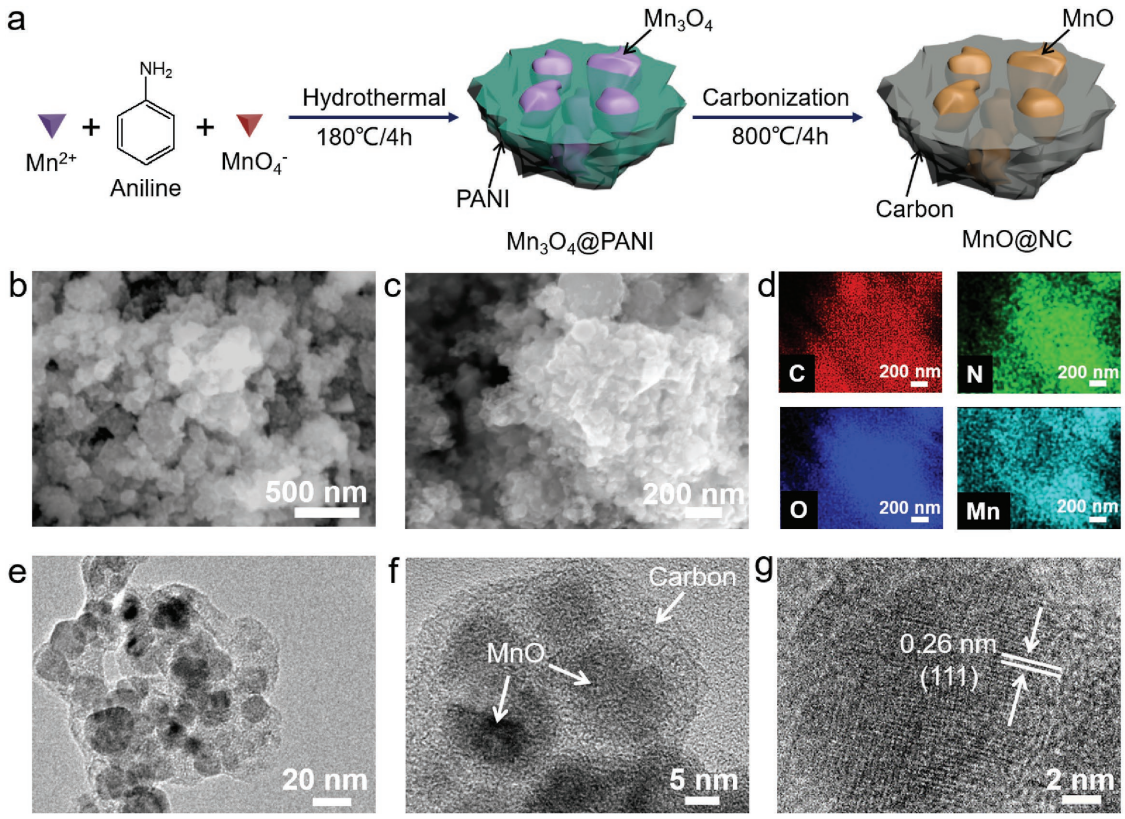

Figure 1. a) Schematic illustration of the preparation process of MnO@NC nanocapsules. b) SEM image of Mn_3O_4@PANI nanocapsules as the intermediate product. c,d) SEM image and elemental mappings (C, N, O, and Mn elements) of MnO@NC nanocapsules. e–g) TEM and HRTEM images of MnO@NC nanocapsules.

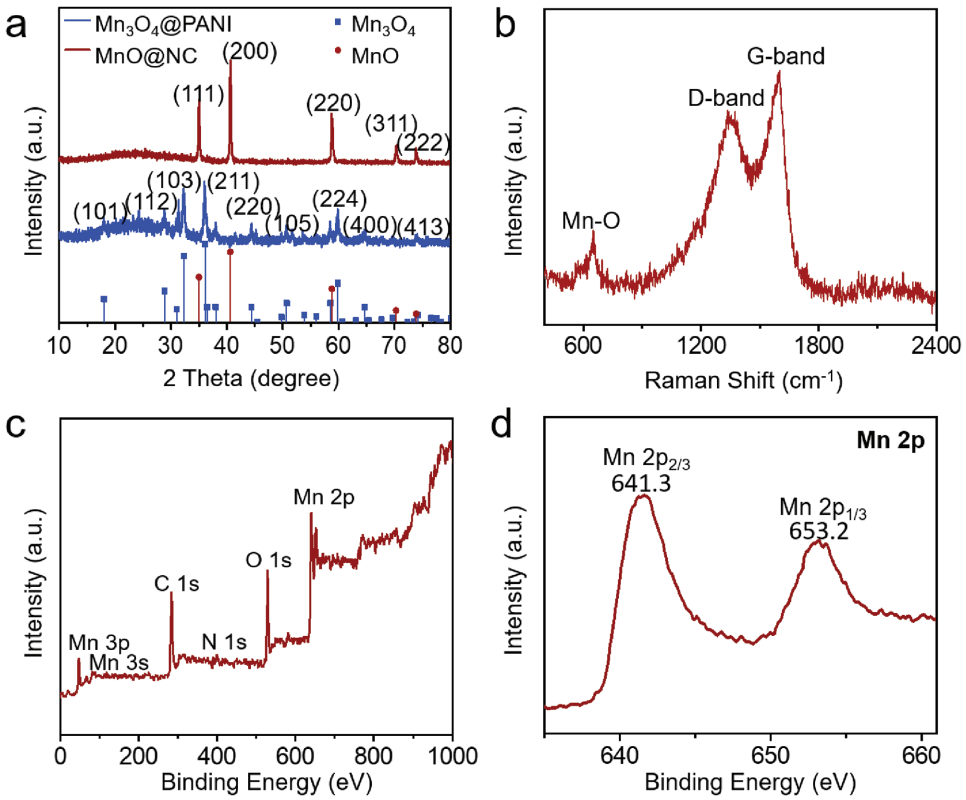

Figure 2. a) XRD patterns of Mn_3O_4@PANI intermediate product and MnO@NC nanocapsules. b) Raman spectrum, c) survey XPS spectrum, and d) high-resolution Mn 2p XPS spectrum of MnO@NC nanocapsules.

nature. After carbonization in N_2 atmosphere, the MnO@NC nanocapsules exhibited strong diffraction peaks at 34.9°, 40.6°, 58.8°, 70.2°, and 73.9°, which were indexed to the (111), (200), (220), (311), and (222) crystal planes of cubic phase MnO (JCPDS No. 75–0626).[26] The diffraction hump between 20° and 30° was attributed to the N-doped carbon shells. In addition, a broad diffraction peak observed from HCl-etched control sample was ascribed to the (002) planes of hollow N-doped carbon nanoshells (Figure S1, Supporting Information). All of these results indicate that the Mn_3O_4@PANI nanocapsules were turned to MnO@NC nanocapsules, and the MnO nanoparticles were well dispersed in the carbon nanoshells. Raman spectroscopy was conducted to evaluate the graphitization degree of carbon nanoshells, as shown in Figure 2b. Two broad Raman peaks at around 1335 and 1589 cm^{-1} were assigned to the D and G bands of partially graphitized carbon, respectively.[32] The intensity ratio of D and G bands (I_D/I_G) was calculated to be 0.91, suggesting the presence of structural distortion caused by defects and N-doping. In addition, a small Raman band was found at 644 cm^{-1}, which was ascribed to the Mn-O vibration of MnO.[27,33] Figure S2 (Supporting Information) shows the Fourier transform infrared spectrum of MnO@NC nanocapsules, exhibiting a strong absorption band at 1610 cm^{-1} originated from the C=C stretching vibration.[34] The absorption bands at 1371 and 1246 cm^{-1} were assigned to the C—N and C—O stretching vibrations,[35,36] respectively. In addition, a weak band corresponding to the Mn—O—C bonds appeared at 1112 cm^{-1},[19] suggesting the physicochemical interaction between MnO nanoparticles and carbon shells. Thermogravimetric analysis (TGA) indicates that the weight content of MnO in MnO@NC nanocapsules is about 79.6% (Figure S3, Supporting Information).

X-ray photoelectron spectroscopy (XPS) was used to clarify the compositions of MnO@NC nanocapsules. The survey XPS spectrum (Figure 2c) implies the presence of Mn, O, C, and N elements. The high-resolution XPS spectrum at Mn 2p region (Figure 2d) exhibits two characteristic peaks at 641.3 eV (Mn $2p_{3/2}$) and 653.2 eV (Mn $2p_{1/2}$) with an energy difference of 11.9 eV. This result is another proof for the formation of MnO.[26,37] The C 1s XPS spectrum of MnO@NC nanocapsules can be deconvoluted into four energy bands located at 284.6, 285.8, 286.7, and 288.6 eV (Figure S4a, Supporting Information), corresponding to C=C, C—N, C—O—C, and C—O, respectively.[38] The N 1s peak (Figure S4b, Supporting Information) can be resolved into three peaks centered at 398.2, 400.5, and 402.0 eV, attributed to the pyridinic-N, pyrrolic-N, and graphitic-N, respectively.[32,39,40] According to the XPS analysis, the contents of C, N, Mn, and O elements in MnO@NC nanocapsules are measured to be 20.5, 1.4, 58.3, and 19.8 wt%, respectively, which are comparable to the TGA (Figure S3, Supporting Information) and EDX results (Figure S5, Supporting Information). The incorporation of N element in carbon framework can enhance the electrical conductivity and provide more active sites for Li^+ insertion.[41–43] To investigate the specific surface area and pore-size distribution of MnO@NC nanocapsules, nitrogen adsorption/desorption isotherms were measured. As

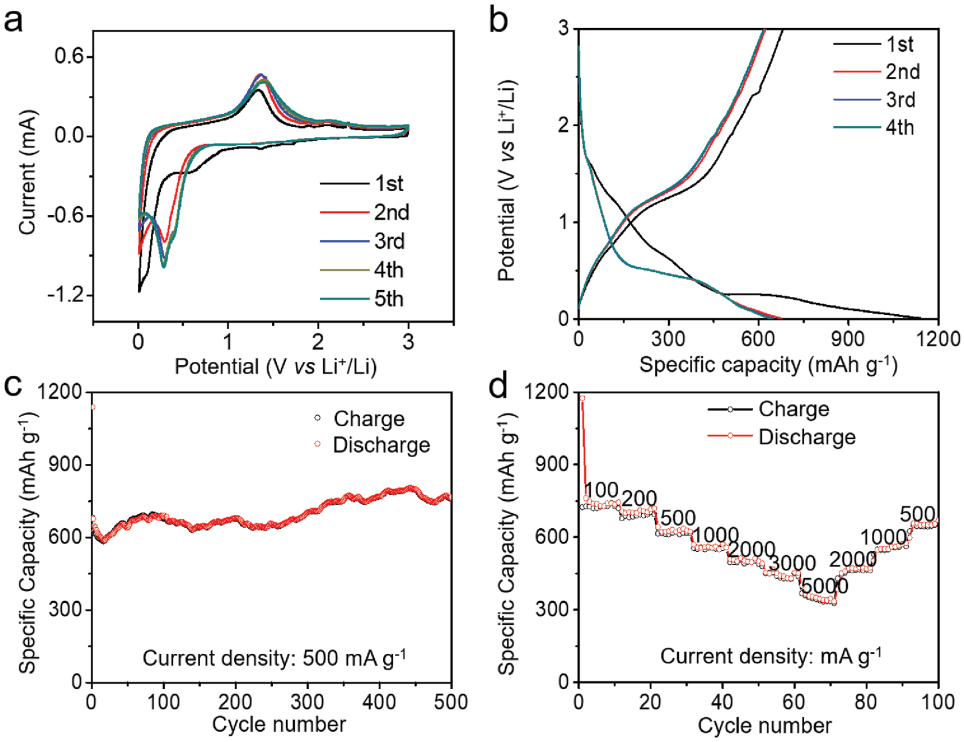

Figure 3. Electrochemical performances of MnO@NC nanocapsules as anode material for LIBs. a) CV curves at a scan rate of 0.2 mV s^{-1} within a potential window of 0.01–3.0 V versus Li/Li^+. b) Discharge/charge curves at a current density of 500 mA g^{-1}. c) Cyclic performance at 500 mA g^{-1}. d) Rate capability in a range from 100 to 5000 mA g^{-1}.

shown in Figure S6a (Supporting Information), the isotherms of MnO@NC nanocapsules display a typical type I shape, and the specific surface area calculated by Brunauer–Emmett–Teller method is 125.2 m^2 g^{-1} with a corresponding pore volume of 0.17 cm^3 g^{-1}. The pore-size distribution of MnO@NC nanocapsules is displayed in Figure S6b (Supporting Information), revealing the abundant micropores centered at 0.6 nm.

The electrochemical performances of MnO@NC nanocapsules as anode material for LIBs are displayed in **Figure 3**. As shown in Figure 3a, cyclic voltammetry (CV) tests were performed to characterize the electrochemical behaviors in a voltage window from 0.01 to 3.0 V versus Li^+/Li at a scan rate of 0.2 mV s^{-1}. In the first cathodic scan, the dominant cathodic peak at 0.11 V corresponds to the initial reduction of MnO to metallic Mn ($MnO + 2Li^+ + 2e^- \rightarrow Mn + Li_2O$).[20,44] Another cathodic peak at 0.59 V was attributed to the formation of solid electrolyte interphase (SEI) layer.[42] Note that a weak cathodic peak emerged at ≈1.36 V in the first cycle, which was assigned to the reduction of higher oxidation state manganese (e.g., Mn^{3+}, Mn^{4+}) originating from the trace Mn_xO_y impurities in MnO.[45] For the first anodic scan, a cathodic peak centered at ≈1.35 V was observed, representing the reversible oxidization of Mn to MnO ($Mn + Li_2O \rightarrow MnO + 2Li^+ + 2e^-$).[44] In the subsequent CV cycles, the reduction peak at 0.11 V shifted to about 0.31 V, suggesting the improved kinetics and the stabilization of SEI layer after the first lithiation process.[20,46]

Figure 3b shows typical galvanostatic discharge/charge curves for the initial four cycles of MnO@NC nanocapsules at a current density of 500 mA g^{-1}. In the first cycle, the MnO@NC nanocapsules delivered a high initial discharge capacity of 1139.4 mAh g^{-1} and a charge capacity of 682.1 mAh g^{-1}. The irreversible capacity loss was mainly attributed to the formation of SEI film, which was common to most of anode materials. During the initial discharge process, a voltage plateau at ≈0.23 V was observed, associated with the reduction of Mn^{2+} to Mn. For the first charge process, a slope between 1.0 and 1.8 V was ascribed to the oxidation of Mn to Mn^{2+}. Starting from the second cycle, the discharge plateau shifted to about 0.49 V due to the enhanced kinetics and the formation of metal nanoparticles and Li_2O.[26]

The cycling stability of MnO@NC nanocapsules at a current density of 500 mA g^{-1} over 500 cycles was illustrated in Figure 3c. The MnO@NC nanocapsules exhibited good cycling performance with a discharge capacity of 767 mAh g^{-1} after 500 cycles. Notably, the specific capacity of MnO@NC nanocapsules after long-term cycling was higher than the theoretical capacities of MnO (756 mAh g^{-1}). This phenomenon could be explained by the activation process, where an electrochemically active gel-like polymeric layer was grown and the oxidation state of manganese changed from Mn^{2+} to a higher oxidation state (Mn^{4+}) during discharge/charge processes.[26,27]

The rate performance of MnO@NC nanocapsules is shown in Figure 3d. The discharge capacities of MnO@NC nanocapsules were 762, 707, 643, 570, 512, and 454 mAh g^{-1} at current densities of 100, 200, 500, 1000, 2000, and 3000 mA g^{-1}, respectively. Even at high current density of 5000 mA g^{-1}, the MnO@NC nanocapsules still delivered a high discharge capacity of 358 mAh g^{-1}. When the current density was restored

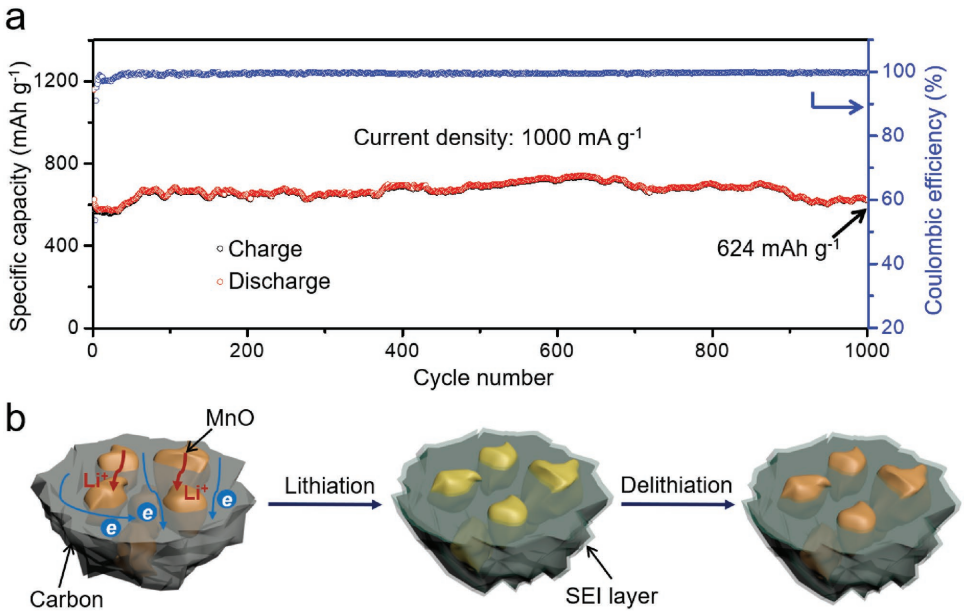

Figure 4. a) Long-term cycling stability of MnO@NC nanocapsules at 1000 mA g^{-1} for 1000 cycles. d) Schematic illustration of walnut-like multicore–shell MnO@NC nanocapsules during lithiation/delithiation processes.

to 500 mA g^{-1}, the discharge capacity recovered to 658 mAh g^{-1}, suggesting that the MnO@NC nanocapsules have intrinsic merits for smooth Li^+ insertion/extraction owing to the synergistic effect of ultrafine MnO cores and conductive carbon nanoshells.[27,46]

Volumetric-specific capacity is another critical parameter for electrode materials. The thickness of MnO@NC nanocapsules electrode with a mass loading of 1.0 mg cm^{-2} was measured to be 8.43 µm. Therefore, the volumetric-specific capacity of MnO@NC nanocapsules was calculated to be 904 mAh cm^{-3} at the current density of 100 mA g^{-1}, which is about two times higher than graphite-based electrode (441 mAh cm^{-3}).[47] This result is also competitive among other anode materials (Table S1, Supporting Information).[48–52]

The MnO@NC nanocapsules also show excellent cycling performance. The discharge capacities and Coulombic efficiencies of MnO@NC nanocapsules at high current density of 1000 mA g^{-1} for 1000 cycles are shown in **Figure 4**a. The initial discharge and charge capacity of MnO@NC nanocapsules were 1159 and 621 mAh g^{-1}, respectively. The discharge capacity increased to 730 mAh g^{-1} at around 600 cycles. Note that the capacity increase phenomenon was similar to that in the cycling tests at 500 mA g^{-1} (Figure 3c), which also could be ascribed to the activation process mentioned above. After cycling for 1000 times, the MnO@NC nanocapsules still delivered a stable discharge capacity as high as 624 mAh g^{-1}, showing high-capacity retention with a Coulombic efficiency of nearly 100%. Compared with other previously reported MnO-based anode materials, the walnut-like multicore–shell MnO@NC nanocapsules exhibited remarkable cycling stability, as summarized in Table S2 (Supporting Information).[20,42–44,52–60]

Based on the above analysis and results, it can be concluded that the outstanding cycling stability of MnO@NC nanocapsules is closely associated with its advantageous structural features, as illustrated in Figure 4b. The walnut-like multicore–shell structure can shorten the Li^+ diffusion pathway and facilitate the Li^+ diffusion during cycling. Moreover, the N-doped carbon nanoshells enable the formation of SEI layer out of the nanocapsules rather than on the MnO/electrolyte interface; therefore, the cycling stability can be improved. For further evidences, SEM and TEM characterizations of MnO@NC electrodes at the full-lithiation state after 1000 cycles at 1000 mA g^{-1} were performed (Figure S7, Supporting Information). The overall morphology was still maintained without obvious structural variation, and the MnO nanoparticles and carbon nanoshells could be clearly identified (Figure S6b, Supporting Information), indicating the high structural integrity after long-term cycling. The electrochemical impedance spectra of MnO@NC nanocapsules before and after 1000 cycles were further investigated, as shown in Figure S8 (Supporting Information). All Nyquist plots displayed a depressed semicircle in the high to medium frequency region, which was related to charge-transfer resistance. The charge-transfer resistance only showed a slight increase before (71.7 Ω) and after cycling (116.3 Ω), demonstrating the good conductivity and structural stability of MnO@NC nanocapsules. Moreover, the cycling performance of MnO@NC electrode with a high mass loading of 2.0 mg cm^{-2} at the current density of 1000 mA g^{-1} is depicted in Figure S9 (Supporting Information). After 100 cycles, the MnO@NC nanocapsules still could deliver a high discharge capacity of 497 mAh g^{-1}, corresponding to a capacity retention of 82.4% relative to the discharge capacity of the second cycle, indicating the good cycle stability of thick electrodes based on MnO@NC nanocapsules.

By using the MnO@NC nanocapsules as anode material, we further construct soft-packed batteries to demonstrate its feasibility. **Figure 5**a shows the schematic configuration of the soft-packed Li-ion cells, mainly composed

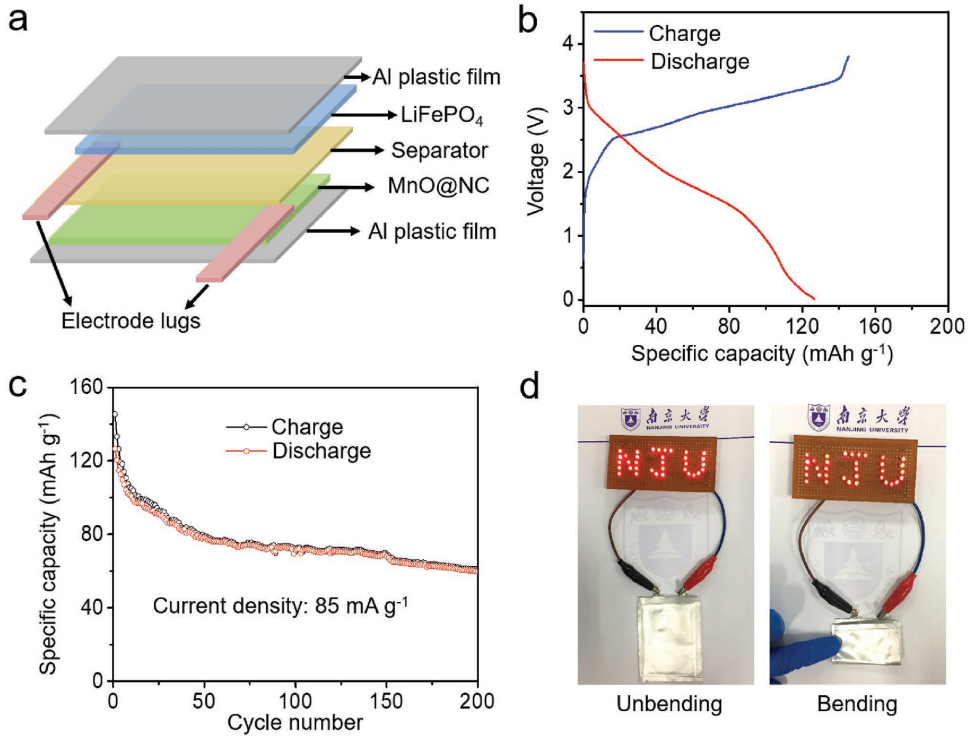

Figure 5. a) Schematic illustration of a soft-packed full battery assembled using MnO@NC nanocapsules loaded Cu foil as the anode and commercial $LiFePO_4$ loaded Al foil as the cathode. b) Discharge/charge curves at a current density of 85 mA g^{-1}. c) Cycling performance of the soft-packed full battery. d) Optical images showing an NJU logo consisting of 34 red LEDs simultaneously powered by the soft-packed battery under continuous bending (folding) and unbending operations.

of MnO@NC nanocapsules based anode, commercial $LiFePO_4$-based cathode, and Celgard separator. Figure 5b presents the discharge/charge curves of the full battery at 85 mA g^{-1} in the voltage window of 0.01–3.8 V. The specific capacity was calculated based on the mass of $LiFePO_4$ because the full battery was cathode limited. The soft-packed battery delivered an initial discharge and charge capacities of 127 and 145 mAh g^{-1}, respectively. The full battery exhibited good stability with a remained specific capacity of 60 mAh g^{-1} after 200 cycles (Figure 5c). Encouragingly, the as-assembled MnO@NC||$LiFePO_4$ full battery can easily power an NJU logo consisting of 34 red light-emitting diodes (LEDs), even under continuous bending (folding) and unbending operations (Figure 5d and Video S1, Supporting Information), verifying its good flexibility.

3. Conclusion

In summary, here we propose a facile strategy to prepare walnut-like multicore–shell MnO@NC nanocapsules with high performance as anode material for LIBs. Benefited from the conductive carbon nanoshells that uniformly encapsulate ultrafine MnO nanoparticles, the electron/ion transfer kinetics and structural stability during discharge/charge cycles can be greatly improved. When used as anode material in LIBs, the MnO@NC nanocapsules showed remarkable discharge capacity retention (624 mAh g^{-1} at 1000 mA g^{-1} after 1000 cycles). Furthermore, the soft-packed MnO@NC||$LiFePO_4$ full battery showed good stability and high flexibility. Such superior electrochemical properties demonstrate that the integration of ultrafine metal oxide nanoparticles and N-doped carbon nanocapsules is an efficient method to improve the performance of metal oxide-based anode materials. This work provides a straightforward and feasible approach for preparing composite electrode materials for long-cycling LIBs.

Supporting Information

Supporting Information is available from the Wiley Online Library or from the author.

Acknowledgements

G.Z. and L.W. contributed equally to this work. This work was supported by National Key R&D Program of China (2017YFA0208200, 2016YFB0700600, and 2015CB659300), Projects of NSFC (21403105, 21573108, and 51761135104), Natural Science Foundation of Jiangsu Province (BK20150583, BK20170644), and the Fundamental Research Funds for the Central Universities (020514380107).

Conflict of Interest

The authors declare no conflict of interest.

Keywords

flexible soft-packed pouch cells, lithium-ion batteries, manganese monoxide nanoparticles, nitrogen-doped carbon nanocapsules, walnut-like multicore–shell composite structures

Received: January 1, 2018
Revised: February 10, 2018
Published online: March 12, 2018

[1] J. M. Tarascon, M. Armand, *Nature* **2001**, *414*, 359.
[2] B. Dunn, H. Kamath, J. M. Tarascon, *Science* **2011**, *334*, 928.
[3] C. K. Chan, H. L. Peng, G. Liu, K. McIlwrath, X. F. Zhang, R. A. Huggins, Y. Cui, *Nat. Nanotechnol.* **2008**, *3*, 31.
[4] D. Larcher, J. Tarascon, *Nat. Chem.* **2014**, *7*, 19.
[5] Y. Wang, R. Chen, T. Chen, H. Lv, G. Y. Zhu, L. B. Ma, C. Wang, Z. Jin, J. Liu, *Energy Storage Mater.* **2016**, *4*, 103.
[6] H. Wu, G. Chan, J. W. Choi, I. Ryu, Y. Yao, M. T. McDowell, S. W. Lee, A. Jackson, Y. Yang, L. Hu, Y. Cui, *Nat. Nanotechnol.* **2012**, *7*, 310.
[7] B. Luo, B. Wang, X. Li, Y. Jia, M. Liang, L. Zhi, *Adv. Mater.* **2012**, *24*, 3538.
[8] N. Liu, Z. Lu, J. Zhao, M. T. McDowell, H. W. Lee, W. Zhao, Y. Cui, *Nat. Nanotechnol.* **2014**, *9*, 187.
[9] Y. M. Cheng, X. Y. Yu, Z. Li, U. Paik, X. W. Lou, *Sci. Adv.* **2016**, *2*, e1600021.
[10] X. Li, J. Zai, S. Xiang, Y. Liu, X. He, Z. Xu, K. Wang, Z. Ma, X. Qian, *Adv. Energy Mater.* **2016**, *6*, 1601056.
[11] C. Xu, Y. Zeng, X. Rui, N. Xiao, J. Zhu, W. Zhang, J. Chen, W. Liu, H. Tan, H. H. Hng, Q. Yan, *ACS Nano* **2012**, *6*, 4713.
[12] P. Poizot, S. Laruelle, S. Grugeon, L. Dupont, J. M. Tarascon, *Nature* **2000**, *407*, 496.
[13] Z. Wang, L. Zhou, X. W. Lou, *Adv. Mater.* **2012**, *24*, 1903.
[14] M. Reddy, G. V. Subba Rao, B. Chowdari, *Chem. Rev.* **2013**, *113*, 5364.
[15] K. Liang, L. Li, Y. Yang, *ACS Energy Lett.* **2017**, *2*, 373.
[16] C. X. Guo, M. Wang, T. Chen, X. W. Lou, C. M. Li, *Adv. Energy Mater.* **2011**, *1*, 736.
[17] J. Gao, M. A. Lowe, H. D. Abruna, *Chem. Mater.* **2011**, *23*, 3223.
[18] J. Guo, Q. Liu, C. Wang, M. R. Zachariah, *Adv. Funct. Mater.* **2012**, *22*, 803.
[19] S. Zhang, L. Zhu, H. Song, X. Chen, J. Zhou, *Nano Energy* **2014**, *10*, 172.
[20] H. Jiang, Y. Hu, S. Guo, C. Yan, P. S. Lee, C. Li, *ACS Nano* **2014**, *8*, 6038.
[21] H. Wang, L. Cui, Y. Yang, H. S. Casalongue, J. T. Robinson, Y. Liang, Yi. Cui, H. Dai, *J. Am. Chem. Soc.* **2010**, *132*, 13978.
[22] X. Li, D. Li, Li. Qiao, X. Wang, X. Sun, P. Wang, D. He, *J. Mater. Chem.* **2012**, *22*, 9189.
[23] Y. Ren, A. R. Armstrong, F. Jiao, P. G. Bruce, *J. Am. Chem. Soc.* **2010**, *132*, 996.
[24] X. Li, X. Shang, D. Li, H. Yue, S. Wang, L. Qiao, D. He, *Part. Part. Syst. Charact.* **2014**, *31*, 1001.
[25] Z. Cui, X. Guo, H. Li, *J. Power Sources* **2013**, *244*, 731.
[26] Y. Xiao, X. Wang, W. Wang, D. Zhao, M. Cao, *ACS Appl. Mater. Interfaces* **2014**, *6*, 2051.
[27] Y. Zhang, P. Chen, X. Gao, B. Wang, H. Liu, H. Wu, H. K. Liu, S. Dou, *Adv. Funct. Mater.* **2016**, *26*, 7754.
[28] V. Etacheri, G. A. Seisenbaeva, J. Caruthers, G. Daniel, J. M. Nedelec, V. G. Kessler, V. G. Pol, *Adv. Energy Mater.* **2015**, *5*, 1401289.
[29] R. Liu, L. Ma, G. Niu, X. Li, E. Li, Y. Bai, G. Yuan, *Adv. Funct. Mater.* **2017**, *27*, 1701635.
[30] T. Chen, Y. Hu, B. Cheng, R. Chen, H. L. Lv, L. B. Ma, G. Y. Zhu, Y. R. Wang, C. Yan, Z. Tie, Z. Jin, J. Liu, *Nano Energy* **2016**, *20*, 305.
[31] F. Han, D. Li, W. C. Li, C. Lei, Q. Sun, A. H. Lu, *Adv. Funct. Mater.* **2013**, *23*, 1692.
[32] G. Y. Zhu, T. Chen, Y. Hu, L. B. Ma, R. P. Chen, H. L. Lv, Y. R. Wang, J. Liang, X. Li, C. Yan, H. Zhu, H. Liu, Z. Tie, Z. Jin, J. Liu, *Nano Energy* **2017**, *33*, 229.
[33] C. Yang, Q. Gao, W. Tian, Y. Tan, T. Zhang, K. Yang, L. Zhu, *J. Mater. Chem. A* **2014**, *2*, 19975.
[34] A. Kuznetsova, D. B. Mawhinney, V. Naumenko, J. T. Yates Jr., J. Liu, R. E. Smalley, *Chem. Phys. Lett.* **2000**, *321*, 292.
[35] J. Zhu, J. He, *ACS Appl. Mater. Interfaces* **2012**, *4*, 1770.
[36] H. W. Wang, Z. A. Hu, Y. Q. Chang, Y. L. Chen, H. Y. Wu, Z. Y. Zhang, Y. Y. Yang, *J. Mater. Chem.* **2011**, *21*, 10504.
[37] C. Liu, C. Zhang, H. Song, C. Zhang, Y. Liu, X. Nan, G. Cao, *Nano Energy* **2016**, *22*, 290.
[38] X. Gu, J. Yue, L. Chen, S. Liu, H. Xu, J. Yang, Y. Qian, X. Zhao, *J. Mater. Chem. A* **2015**, *3*, 1037.
[39] D. Wei, Y. Liu, Y. Wang, H. Zhang, L. Huang, G. Yu, *Nano Lett.* **2009**, *9*, 1752.
[40] W. Niu, Z. Li, K. Marcus, L. Zhou, Y. Li, R. Ye, K. Liang, Y. Yang, *Adv. Energy Mater.* **2018**, *8*, 1701642.
[41] K. N. Wood, R. O'Hayre, S. Pylypenko, *Energy Environ. Sci.* **2014**, *7*, 1212.
[42] L. F. Chen, S. X. Ma, S. Lu, Y. Feng, J. Zhang, S. Xin, S. H. Yu, *Nano Res.* **2017**, *10*, 1.
[43] W. Zhang, J. Sheng, J. Zhang, T. He, L. Hu, R. Wang, L. Q. Mai, S. Mu, *J. Mater. Chem. A* **2016**, *4*, 16936.
[44] H. Liu, Z. Li, Y. Liang, R. Fu, D. Wu, *Carbon* **2015**, *84*, 419.
[45] W. Chen, L. Qie, Y. Shen, Y. M. Sun, L. X. Yuan, X. L. Hu, W. X. Zhang, Y. H. Huang, *Nano Energy* **2013**, *2*, 412.
[46] W. Zhang, J. Li, J. Zhang, J. Sheng, T. He, M. Tian, Y. Zhao, C. Xie, L. Mai, S. Mu, *ACS Appl. Mater. Interfaces* **2017**, *9*, 12680.
[47] S. Jeong, J. P. Lee, M. Ko, G. Kim, S. Park, J. Cho, *Nano Lett.* **2013**, *13*, 3403.
[48] Q. Xiao, Y. Fan, X. Wang, R. A. Susantyoko, Q. Zhang, *Energy Environ. Sci.* **2014**, *7*, 655.
[49] E. M. Lotfabad, J. Ding, K. Cui, A. Kohandehghan, W. P. Kalisvaart, M. Hazelton, D. Mitlin, *ACS Nano* **2014**, *8*, 7115.
[50] T. Ma, X. Yu, H. Li, W. Zhang, X. Cheng, W. Zhu, X. Qiu, *Nano Lett.* **2017**, *17*, 3959.
[51] J. Liu, J. Wang, J. Kim, H. Ning, Z. Pan, S. J. Kelly, E. S. Epstein, X. Huang, J. Liu, P. V. Braun, *Small* **2015**, *11*, 6265.
[52] L. Sheng, S. Liang, T. Wei, J. Chang, Z. Jiang, L. Zhang, Q. Zhou, J. Zhou, L. Jiang, Z. Fan, *Energy Storage Mater.* **2018**, *12*, 94.
[53] H. Hu, H. Cheng, Z. Liu, Y. Hu, *Electrochim. Acta* **2015**, *152*, 44.
[54] X. Zhang, Z. Xing, L. L. Wang, Y. C. Zhu, Q. W. Li, J. W. Liang, Y. Yu, T. Huang, K. B. Tang, Y. T. Qian, X. Y. Shen, *J. Mater. Chem.* **2012**, *22*, 17864.
[55] X. Fan, S. Li, L. Lu, *Electrochim. Acta* **2016**, *200*, 152.
[56] L. Zhang, D. Ge, G. Qu, J. Zheng, X. Cao, H. Gu, *Nanoscale* **2017**, *9*, 5451.
[57] Q. Zhang, Q. Dai, M. Li, X. Wang, A. Li, *J. Mater. Chem. A* **2016**, *4*, 19132.
[58] J. G. Wang, C. B. Zhang, D. D. Jin, K. Y. Xie, B. Q. Wei, *J. Mater. Chem. A* **2015**, *3*, 13699.
[59] M. Zhong, D. Yang, C. Xie, Z. Zhang, Z. Zhou, X. H. Bu, *Small* **2016**, *12*, 5564.
[60] H. Wei, Z. Xia, D. Xia, *ACS Appl. Mater. Interfaces* **2017**, *9*, 43657.